

Cascades in nonlocal turbulence

Gregory Falkovich^{1,2} and Natalia Vladimirova³

¹*Weizmann Institute of Science, Rehovot 76100 Israel*

²*Institute for Information Transmission Problems, Moscow, 127994 Russia*

³*University of New Mexico, Department of Mathematics and Statistics, Albuquerque NM 87131*

(Dated: March 7, 2022)

We consider developed turbulence in 2d Gross-Pitaevsky model, which describes wide classes of phenomena, from cold atoms and optics to condensed matter, fluids and plasma. Well-known difficulty of the problem is that the hypothetical local spectra of both inverse and direct cascades in weak-turbulence approximation carry fluxes which either is zero or has a wrong sign; such spectra cannot be realized. We derive analytically the exact flux constancy laws (analogs of Kolmogorov's 4/5-law for incompressible fluid turbulence), expressed via the fourth-order moment and valid for any nonlinearity. We confirmed the flux laws in direct numerical simulations. We show that a constant flux is realized by non-local wave interaction both in direct and inverse cascades. Wave spectra (second-order moments) are close to slightly (logarithmically) distorted thermal equilibrium in both cascades.

I. INTRODUCTION

Turbulence is a state where pumping and dissipation happen at very different scales, so that the main issue is the nature of the transfer of a conserved quantity (say, energy) from pumping to damping due to nonlinear interaction. Despite the fundamental importance of this process, there is a certain terminological (and even conceptual) confusion surrounding the notion of locality of turbulence cascades. It may seem clear intuitively: either the energy is transferred locally in k -space by a cascade-like process or jumps directly from the motions of pumping scales to those of damping scales.

The problems start when one tries to sort out how formally locality or non-locality is manifested in the correlation functions. The simplest case is that of a complete scale invariance when the statistics at the scales between the pumping scale l_p and the damping scale l_d are independent of l_p and l_d ; it is then natural to call it a local cascade. Such cases do exist, as, for instance, an inverse energy cascade in 2d incompressible turbulence [1], where the velocity structure functions have normal scaling: $\langle |v(r) - v(0)|^n \rangle \propto r^{n/3}$. However, scale invariance is spontaneously broken in the direct cascades, see e.g. [2]. Indeed, the direct energy cascade in 3d have l_p explicitly entering all the velocity structure functions except the third, which determines the energy flux through the scale r . The same is true for the direct vorticity cascade, where all velocity and vorticity correlation functions contain l_p , again, except the triple moment expressing the flux of squared vorticity [3–5]. Are we to call such turbulence non-local, because the pumping scale explicitly determines the moments (including the second one i.e. the energy spectrum), or to classify it as a local cascade, because the flux through the scales is constant?

Even more confusion one finds in weak turbulence theory, which aspires to provide a close description solely in terms of the second moment – if it contains l_p and/or l_d , turbulence is called non-local [6]. We wish to state here that even in such cases there must exist a higher-

order correlation function which is universal i.e. dependent neither on l_p, l_d nor on mechanisms of pumping and dissipation.

It is thus important to clearly distinguish non-locality of turbulence (when some correlation functions in the inertial interval depend on pumping and/or dissipation scale) and locality of the flux, which corresponds to a single correlation function independent of l_p and l_d . Locality of the flux is, in a sense, trivial consequence of a conservation law, and it may co-exist with non-locality of turbulence.

Here we show that such co-existence takes place for 2D turbulence in the framework of Gross-Pitaevsky model. We derive universal (i.e. independent of l_p, l_d) flux relations both for direct and inverse cascades. Those universal flux relations are expressed via the fourth moments. And yet we show that both cascades are not scale-invariant, so that the second moments (and spectral densities) explicitly depend on pumping and dissipation scales.

II. FORMULATION OF PROBLEM

The Gross-Pitaevsky model is one of the most universal models in physics. It describes wave propagation in wide classes of phenomena in fluids, solids and plasma. Applications include light propagating in media with the Kerr nonlinearity [7], and non-equilibrium states of cold atoms in Bose-Einstein condensates [8].

The range of applications is broad because the physical model is build on a single assumption: narrow distribution in the space of momenta of wave vectors. The complex wave envelope ψ evolves then according to Gross-Pitaevskii, or nonlinear Schrodinger equation,

$$\psi_t = i\nabla^2\psi + is|\psi|^2\psi. \quad (1)$$

In the right-hand side, the first term describes a linear propagation, and the second term represents non-linear interaction (of waves or particles). The param-

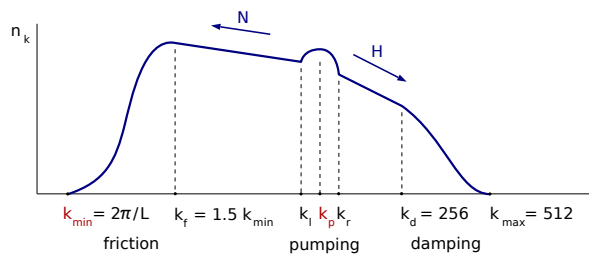


FIG. 1: Schematic representation of forcing and damping in spectral space

eter s in front of the nonlinear term distinguishes the focusing/attractive ($s = +1$) and defocusing/repulsive ($s = -1$) cases.

The equation (1) has two integrals of motion (conserved quantities): the wave action, $\mathcal{N} = \int |\psi|^2 d\mathbf{r}$, and the Hamiltonian, $\mathcal{H} = \int |\nabla\psi|^2 - \frac{1}{4}s|\psi|^4 d\mathbf{r}$. Assuming a weak nonlinearity, it can be shown that the cascade of wave action in spectral space is inverse [6], i.e. directed toward small wave numbers, while the cascade of the energy is direct. Independently of the sign of nonlinearity, the inverse cascade results in the appearance of large, spatially-coherent structures [9, 10], and, in the case of defocusing nonlinearity, in the accumulation of condensate — the mode spatially-coherent across the whole system. In this study, however, we avoid condensate creation by either considering times well before formation of condensate or adding dissipation at low k . Therefore, even though we work with $s = -1$, some of our results could be relevant to the focusing case as well.

We numerically solve the Eq. (1) with defocusing nonlinearity, using a standard split-step method [9] modified to be 4th-order accurate in time. Forcing and damping, applied in spectral space, are represented in the r.h.s. of the equation,

$$i\psi_t + \nabla^2\psi - |\psi|^2\psi = i\hat{f}_k\psi + i\hat{g}_k. \quad (2)$$

Our computational domain is square, $L \times L$, with periodic boundary conditions, so that the lowest wave number is determined by the domain size, $k_{\min} = 2\pi/L$. All simulation presented here are done at the same resolution, $\Delta x = \Delta y = 2\pi/1024$, and time step $\Delta t \leq 10^{-5}$. We use domains up to $L = 32\pi$, with grids up to 16386^2 points.

To deposit wave action into the system we use the additive forcing, $g_k = |g_k|e^{i\phi_k}$, with random phases ϕ_k and amplitudes $|g_k| \propto \sqrt{(k^2 - k_l^2)(k_r^2 - k^2)}$ which are non-zero only in a ring of wavenumbers $k \in [k_l, k_r]$. The forcing is normalized to deposit specified amount of wave action, $\dot{N} \equiv \alpha$, where $N = \int |\psi|^2$ and overline denotes space averaging. The multiplicative forcing, $f_k = -\beta(k/k_d)^4(k/k_d - 1)^2$, provides small scale damping at $k > k_d$. We use $k_d \approx 3k_r$ to include contribution of cubic nonlinearity to direct cascade. In addition to high- k damping, we have an option to include low- k friction, $f_k = -(1, 1, \frac{1}{\sqrt{2}})\gamma$ for $k = (0, 1, \sqrt{2})k_{\min}$. While

dissipation and low and high wavenumbers are described by the same term in the equation, they serve different purposes in our simulations, and further we will refer to them by different names, as “damping” and “friction”. The purpose of friction is to stabilize the spectrum and prevent the accumulation of condensate, while the purpose of damping is to limit the spectrum to finite number of modes.

One advantage of running at the same resolution is that we can use the same damping parameters, $k_d = 256$ and $\beta = 400$, in all simulations. Our studies of the inverse cascade are done with pumping rings with $k_l = 68$ and $k_r = 84$, while our simulations of direct cascade are done with $k_l = 6k_{\min}$ and $k_r = 9k_{\min}$. The strength of forcing and friction are controlled by α and γ respectively, which are treated as simulation parameters.

Notice that α is an input rate of wave action into the system, which is not the same as the flux into the inverse cascade, $\tilde{\alpha}$. In our simulations of inverse cascade at most 10% of wave action is lost to damping, that is $\tilde{\alpha} \gtrsim 0.9\alpha$. The lost fraction is measured by computing the wave action consumed by friction in stabilized simulations, and also from the slope of $N(t)$ in simulations without friction, where the initial slopes match the rates of wave deposition α and switch to $\tilde{\alpha}$ later. These simulations will be discussed in more detail in corresponding sections.

III. FLUX LAWS AS FOURTH MOMENTS

Below we show that flux laws expressed in terms of fourth moments are exact and local, that is independent of k_p and L . Non-locality of second moments, i.e. lack of scale invariance, will be shown in the following sections.

Let us imagine an infinitely large, time-evolving system without friction, and look at the following quantity, $\langle |\psi_1 - \psi_2|^2 \rangle$. Here ψ_1 and ψ_2 refer to the values at two points separated by the distance r taken in the interval of inverse cascade, $L \gg r \gg k_p^{-1}$. Angular brackets refer to the space averaging. Let us assume that the inverse cascade has already passed the scale r , that the statistics of fluctuations at this and smaller scales are stabilized, but larger-scale fluctuations are still growing. We can visualize this as fast-changing, but statistically the same ripples on top of slowly growing and slowly evolving background (Fig. 2). In such system, the average difference $\langle |\psi_1 - \psi_2|^2 \rangle$ remains constant in time, even though each of $\langle |\psi_1| \rangle$ and $\langle |\psi_2| \rangle$ are increasing.

This second moment can be related to the spectral density:

$$\langle |\psi_1 - \psi_2|^2 \rangle = \int |\psi_k|^2 (1 - \cos kr) dk \simeq \int_{1/r}^{\infty} |\psi_k|^2 dk.$$

Next, we use NLSE to take time derivative of

$$\langle |\psi_1 - \psi_2|^2 \rangle = 2N - \langle \psi_1\psi_2^* + \psi_1^*\psi_2 \rangle$$

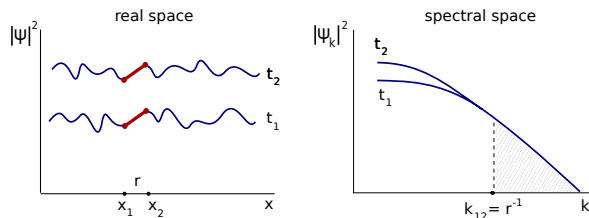


FIG. 2: Invariance of $\langle |\psi_1 - \psi_2|^2 \rangle$ correlation function.

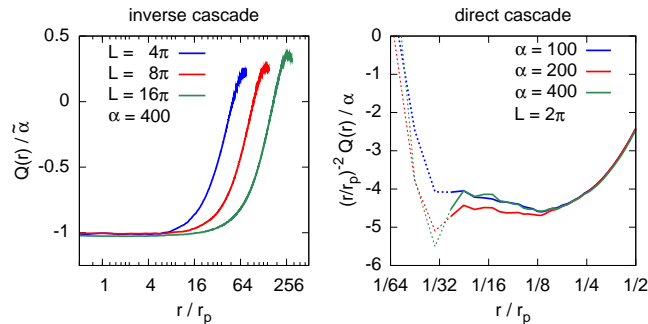


FIG. 3: The ratio of the correlation function $Q(r)$ to the input rate of wave action in simulations of inverse and direct cascades (left and right panels respectively). The data are collected over time and averaged in angular direction. The filter removing harmonics with $k > k_l$ is applied before averaging in the inverse cascade runs. Dashed lines are data in the damping interval of scales.

and obtain,

$$Q(r) \equiv 2 \operatorname{Im} \langle \psi_1^* |\psi_2|^2 \psi_2 \rangle = -\tilde{\alpha}. \quad (3)$$

Note that the right hand side is an outcome of all mechanisms of pumping and dissipation acting at the scales smaller than r , i.e. the effective flux of action into the inverse cascade. This result is non-trivial because it shows that the fourth correlation function $Q(r)$ is the divergence of the wave action flux, which is equal to the input rate in the steady state and thus does not depend on the distance r .

Simulations with different input rates show that $Q(r)$ scales as α in the range from the damping scale to the size of the domain, both for direct and inverse cascades. Simulation of the inverse cascade confirm the appearance of the plateau, $Q(r) = -\tilde{\alpha}$ for $r \gtrsim r_p$, as shown in Fig. 3, left panel. We have filtered out small-scale oscillations $r < r_p$, resulting from spectrally narrow pumping.

For the direct energy cascade, generally one cannot obtain a scale-invariant flux law since the energy contains two terms: quadratic kinetic term $|\nabla\psi|^2$ and quartic potential term $|\psi|^4$. At least for not very strong nonlinearities, when potential energy is not very large, we expect the kinetic energy flux, $P = \nabla^2 Q$, to be scale-independent, or equivalently $Q(r) \sim r^2$. Right panel of

Fig. 3 shows that indeed $Q(r)/\alpha \approx -4.5(r/r_p)^2$, resulting in $P \approx -18 \alpha r_p^{-2}$, for $r \lesssim 0.2 r_p$.

IV. INVERSE CASCADE

Evolution of spectra

We start with the description of the inverse cascade developing without friction. As wave action accumulates in low- k modes, one can distinguish three distinct regimes, with spectra shown in Fig. 4. During the first stage, pumping-related waves grow fast and then start slowly decay towards some lower steady-state value. The early regime is followed by intermediate one with time-dependent energy-action equipartition:

$$n_k = \frac{T(t)}{k_\mu^2(t) + k^2}. \quad (4)$$

Here, T and $\mu \equiv k_\mu^2$ can be interpreted as temperature and chemical potential, both slowly evolving in time. The transition from the first to the second regime happens when k_μ drops below k_p . At later times, the third regime is characterized by the appearance of a ‘‘bottleneck’’ pile-up at lower k and a dip at high k .

The first two stages can be seen as a single process: formation of the turbulence spectrum close to equilibrium both at the scales larger and smaller than the pumping scale. Initially, chemical potential is so large that $k_\mu(t) > k_p$ and most of the waves at $k < k_p$ appear in the state of action equipartition. Filling the system with waves, we decrease the chemical potential; after k_μ decreases below k_p we start seeing the part of energy equipartition $n_k \propto k^{-2}$ simultaneously with the grows of n_k at $k > k_p$.

That form of evolution is already a sign of nonlocality of interaction: instead of a front propagating to lower k , we see simultaneous growth of a wide spectrum over all available wavenumbers to the left of k_p .

The evolution of the temperature and the chemical potential during the second stage is shown in Fig. 5. The temperature drop during the second and the third regimes corresponds to the drop in the level of $n_k \approx T/k^2$ in the power-law part of the spectrum and the expansion of the power-law tail. The lowering of the tail is accompanied by the rise and contraction of the low- k plateau, $n_k \approx T/k_\mu^2$.

One expects the temperature to saturate. Then, the linear growth of the wave action, $\int n_k d\mathbf{k} \approx T \ln(k_p/k_\mu) \simeq \tilde{\alpha} t$, must lead to an exponential decrease of k_μ , which is indeed seen in Fig. 5. Decrease of the chemical potential below $k_\mu = 2$ is accompanied by deviation of spectra from the simple form (4).

One might find the decrease of the temperature $T(t)$, or the magnitude of the spectra in the region $n_k \approx T(t)k^{-2}$, counter-intuitive. We think it can be interpreted again in terms of nonlocal interaction: to carry the fixed flux α by an extended spectrum with higher bump one needs

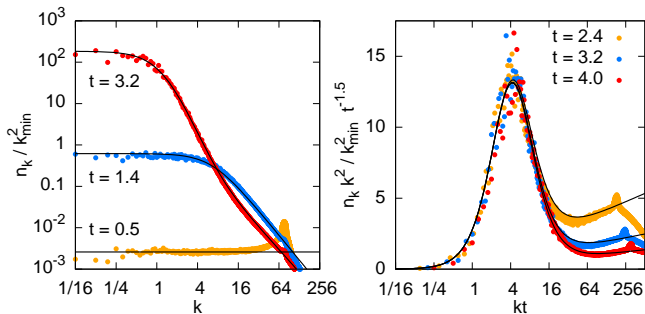


FIG. 4: Left: Early evolution of the spectra without friction for $\alpha = 400$. The lines are fits by Eq. (4) and Eq. (5). Right: The pile-up of wave action at later times can be mapped into a universal curve by rescaling the abscissa and ordinate axes by t and $t^{-1.5}$ respectively. The black lines are fits by Eq. (5) with parameters specified in the text.

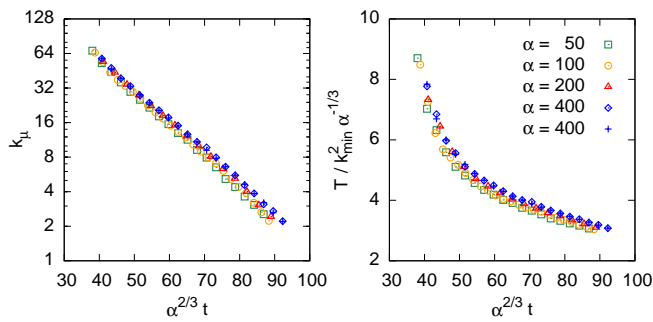


FIG. 5: Chemical potential and temperature during friction-free evolution at intermediate times for different α . Chemical potential decay is close to the exponential fit $k_\mu = Ae^{-\varkappa t}$ with $A = 640$ and $\varkappa = 0.062\alpha^{2/3}$. We see that the temperature T (and then n_k) scales as $\alpha^{1/3}$ while time scales as $\alpha^{-2/3}$. All points, except crosses, are from simulations with $L = 8\pi$; crosses are from simulations with $L = 32\pi$.

smaller amplitude. In other words, nonlocal action transfer through a given k is determined by both an amplitude and an extent of the interval. When the interval expands towards lower k and acquires higher bump at low k , the transfer is getting more effective and the magnitude decreases. It seems that the pile-up is not due to approaching the minimal wavenumber but rather at those k where nonlinearity is getting substantial (this is also supported by the steady-state spectra shown below in Fig 6, where stronger nonlinearity leads to more pile-up at higher nonlinearities even in large boxes; pumping at lower rate α reduces piling-up and extends the spectrum).

The late evolution of spectra is shown in the right panel of Fig. 4. The shape of the spectra can be empirically fit by the following expression:

$$n_k = \frac{T(1 + c_1 c_2 k^2 \ln[kt])}{k_\mu^2 + k^2 + c_2 k^4}, \quad (5)$$

where parameters T , k_μ , c_1 , and c_2 are functions of time. The late-time fits shown in Fig. 4 are done for the simulation with $\alpha = 400$ and correspond to $T/k_{\min}^2 = 24.6 t^{3/2}$, $k_\mu = 2.8 t^{-1}$, $c_2 = 0.025 t^2$, and $c_1 = 0.36 t^{-2.67}$. Note that the effective temperature grows at the late stage. The numerical coefficients in this fit are specific for $\alpha = 400$; spectra for smaller pumping rates develop slower and have less pronounced pile-up due to nonlinearity.

When $c_1 = c_2 = 0$, Eq. (5) is reduced to Eq. (4). The logarithmic correction in the nominator describes the high- k end of the spectrum, while the last term in the denominator accounts for the next order of a low- k expansion in powers of k^2 ; it is needed to describe the pile-up at intermediate k . That is similar to the form

$$n_k = \frac{T}{k_\mu^2 + k^2 + qk^4 \ln^2(k/k_c)}, \quad (6)$$

suggested in [9] with $q \equiv 4aQT^{-3}$. Our simulations do not confirm (6). In the limited range of intermediate wavenumbers we have $q \ln^2(k/k_c) \approx \text{const} = c_2$ rather than the logarithmic dependence, while the high- k asymptotic is dominated by the $c_1 \ln[kt]$ term. Instead of $q \propto T^{-3}$, we observe both c_2 and T (and Tc_1c_2) increasing with time. One should not read too much into non-monotonic time dependence (decay followed by growth) of the parameter T . The late-stage dynamics is consistent with the earlier trend of the decrease of the high- k tail of the spectrum and the growth of the pile-up. In the parametrization (5) the effective temperature rises because it describes the amplitude of the pile-up rather than of the tail, which is governed by $c_1 T \propto t^{-1.17}$.

One conclusion we can draw from the fit is that the location of the pile-up moves to the left as t^{-1} while its amplitude grows as $t^{3/2}$. One may interpret the pile-up as a moving bottleneck [11], which eventually hits the box size. The scalings gives an estimate for the time of formation of condensate in large boxes.

Stabilized spectra

To reach a steady state with a constant flux through a transparency window one turns on low- k friction. We have performed several such simulations with different flux rates and in domains with different sizes.

We characterize the degree of nonlinearity by the ratio of mean potential energy of interaction to the kinetic energy: $H_p/H_k = \langle |\psi|^4 \rangle / \langle |\nabla\psi|^2 \rangle$. In simulations with smaller nonlinearities ($100 \leq \alpha \leq 800$, $0.07 < H_p/H_k < 0.15$) the spectra have the weak-turbulence scaling, $n_k \propto \alpha^{1/3}$ [6], confirming dominance of resonant four-way interactions (see Fig. 6a). The higher- k parts of compensated spectra (to the immediate left of pumping) have a well-defined slope, which can be described by logarithmic correction similar to evolving spectra. This part of the spectra is relatively insensitive to friction. The pile-up at low k is seen as well, but now its amplitude

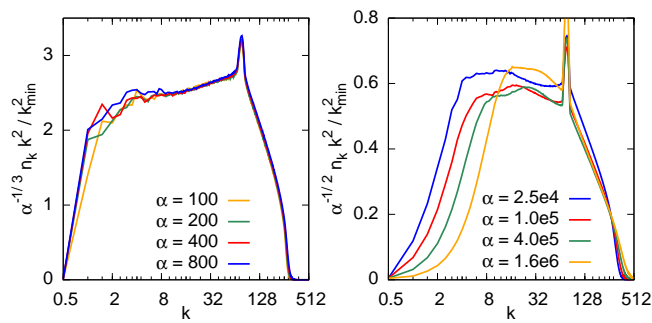


FIG. 6: Effect of pumping rate on stabilized spectra in simulations with $L = 4\pi$. At lower rates $n_k \sim \alpha^{1/3}$ (left panel), while at higher rates $n_k \sim \alpha^{1/2}$ and spectra develop equipartition region (right panel). Friction was selected to minimize the pile-up: $\gamma = 6.2\alpha^{2/3}$ for $\alpha \leq 800$ and $\gamma = (250\alpha)^{1/2}$ for $\alpha \geq 2.5 \times 10^4$.

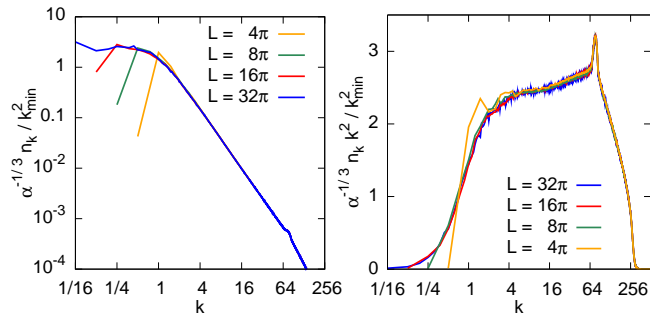


FIG. 7: Spectra in simulations with different domain sizes. In all runs $\alpha = 400$ and $\gamma = 6.2\alpha^{2/3} = 337$.

and location depends on the friction. Adjusting γ we can minimize pile-up, but cannot eliminate it completely.

The pile-up is more pronounced at higher nonlinearities ($2.5 \times 10^4 \leq \alpha \leq 1.6 \times 10^6$, $0.4 < H_p/H_k < 1.5$) completely eliminating the part of the spectrum that logarithmically decreases towards lower k (Fig. 6b). At higher nonlinearities we start to observe the action equipartition as seen in the left panel of Fig 7 for $L = 32\pi$ and in compensated spectra in Fig. 6 as a gap at low k ; the higher α the wider the gap. Unlike the amplitude of pile-up, which is very sensitive to friction, the width of the gap is relatively robust; the friction slightly affects the width of equipartition region, but cannot eliminate it.

At high input rates, the overall level of spectra changes from $n_k \propto \alpha^{1/3}$ scaling to $n_k \propto \alpha^{1/2}$ suggesting transition to three-way interaction, which are non-resonant without a condensate. It could well be that in our case the role of condensate (or “pre-condensate”) play the collection of low- k modes. To analyze the degree of coherence between these modes and their role in interactions with the rest of the spectrum remains a subject for future work.

A pile-up and low- k equipartition, similar to those

shown in Fig. 6, was observed in simulations of water wave turbulence and attributed to the bottleneck [11] due to lack of low-frequency modes [14]. In our case, we can rule out this explanation, since our simulations performed in increasing domains show the appearance of the equipartition region even for moderate α . As shown in Fig. 7, additional low- k modes do not affect the bending point in the spectra. And, as before, the variation of γ distorts the spectra, but cannot eliminate the gap. The consistency of the bending point in simulations of increasing sizes suggests that this is an effect of interaction of low and high- k modes.

V. DIRECT CASCADE: STABILIZED SPECTRA

Next, we take a look at the steady-state spectra of the direct cascade. To do so, we shift the pumping shell to lower modes, $k/k_{\min} = [6, 9]$ while keeping the friction in the interval $[0, k_{\min}]$. We perform simulation with $k_{\min} = 1, 1/2, 1/4$ and with different α . The friction coefficient is selected to minimize the pile-up at low- k . The same simulations were used in the study of energy flux presented earlier.

The typical spectra are shown in Fig. 8. Far from the pumping, the spectra scale as $n_k \propto \alpha^{1/2}$, similarly to inverse cascades with high nonlinearities. As we extend our computational domain we observe a non-universal region at low k and a universal region at high k (in our case, $k > 16$). Next, we compare the shape of the spectra in universal region to the theory by Malkin [12]. The theory assumes non-local weakly-nonlinear interaction and describes the shape of direct cascade in terms of N_k/N , which is the fraction of wave action contained within a sphere of radius k . The spectrum, n_k , is described implicitly through the following equations,

$$\frac{n_k k^2}{k_{\min}^2} = \frac{C}{2\pi} \left[\ln \frac{N}{N_k} \right]^{\frac{1}{3}}, \quad (7)$$

$$\frac{C}{N} \ln \frac{k_M}{k} = p\left(\frac{N_k}{N}\right), \quad (8)$$

where C is a constant related to the energy flux, and k_M is the cut-off mode. The function $p(m)$ is an integral which can be expressed in terms of the lower incomplete gamma function, $\mathcal{P}(a, x)$, e.g. [13] Eq. (6.5.1),

$$p(m) = \int_m^1 \ln^{-\frac{1}{3}} \frac{1}{y} dy = \Gamma\left(\frac{2}{3}\right) \mathcal{P}\left(\frac{2}{3}, \ln \frac{1}{m}\right). \quad (9)$$

To compare our data and the theory predictions, we extract N_k/N from numerical simulations and verify Eq.(7) and Eq.(8) individually. The comparison shows a good agreement in the range $\ln(N/N_k) \in [10^{-3}, 0.3]$, or for $N_k/N \in [0.74, 0.999]$. We stress that the data is fitted with the single parameter, $C = 88$ for $\alpha = 400$. The total wave action, $N = 405$, is computed from simulations. As for the cutoff mode, we use $k_M = 270$, which

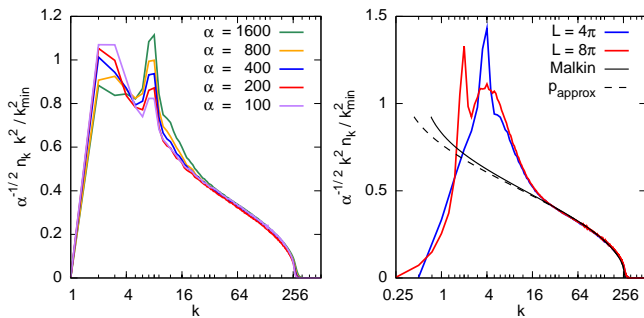


FIG. 8: Left: Spectra of direct cascade for $L = 2\pi$ and different α . Right: Spectra with $\alpha = 400$ compared with Malkin model, fit with $C = 88$. In all runs $\gamma = 6.2\alpha^{\frac{2}{3}}$.

works better than the damping cutoff, $k_d = 256$. Taking into account that damping is a smooth function of k , non-zero at $k \gtrsim k_d$, we find this modification acceptable. Once we have determined parameter C in Eqs.(7)-(8), we can combine these equations to describe the shape of the spectrum in a parametric representation, which makes the black solid curve in Fig. 8b. To provide an explicit expression for $n_k(k)$, one can approximate (9) as $p_{\text{approx}}(m) = \frac{3}{2}(1-m)^{\frac{2}{3}}$ [15], which gives

$$\frac{n_k k^2}{k_{\text{min}}^2} = \frac{C}{2\pi} \ln^{\frac{1}{3}} \left[1 - \left(\frac{2C}{3N} \ln \frac{k_d}{k} \right)^{\frac{3}{2}} \right]. \quad (10)$$

In the range $k \in [16, 256]$ where the original theory agrees with the data, the approximation works as well as the original parametric representation. The agreement of the final expression with the data might not be impressive on its own (for example, $n_k k^2 \propto \ln^{\frac{1}{2}}(k_M/k)$ also provides a good fit), however the agreement of underlying arguments gives additional support to the theory.

Our results can be extended beyond the single value of α , by taking into account $n_k \propto \alpha^{\frac{1}{2}}$ scaling, which leads

to $C = c\alpha^{1/2}$ with $c \approx 4.4$. To connect C to the energy flux, we recall our earlier observation, $P = \nabla^2 Q \propto \alpha$, illustrated in Fig. 3, to conclude that $C \propto P^{1/2}$. This is different from $C \propto P^{1/3}$ proposed by Malkin who assumed weak nonlinearity. Yet nonlinearity restricts the range of applicability of the theory to high- k part of the spectrum. We speculate that the deviation at small k can be reduced, and the range of applicability can be extended, if comparison were done for smaller α .

VI. CONCLUSION

We have suggested and confirmed exact fourth-order flux relations both for direct and inverse cascades. We have found the second moments i.e. the spectra nonlocal for both cascades. The inverse cascade is weakly turbulent at low pumping rates, while nonlinearity is found to be substantial for the direct cascade at any input rate and for the inverse cascade at high input rates.

Acknowledgement

A part of this work was done during the visit to the Kalvi Institute for Theoretical Physics, UCSB, supported by grant no. NSF PHY11-25915. N.V. was in part supported by NSF grant no. DMS-1412140. Simulations were performed at the Center for Advanced Research Computing (CARC), UNM, and Texas Advanced Computing Center (TACC) using Extreme Science and Engineering Discovery Environment (XSEDE), which is supported by NSF grant no. ACI-1053575. G.F. work is supported by grants of Bi-National Science Foundation, Minerva Foundation with funding from the German Ministry for Education and Research and by Russian Science Foundation project No. 14-22-00259 (development of the analytical theory and writing the paper).

-
- [1] G. Boffetta and R. E. Ecke, Annual Review of Fluid Mechanics **44**, 427 (2012).
 - [2] G. Falkovich, J Phys A: Math Theory **42**, 123001 (2009).
 - [3] R. H. Kraichnan, Physical Review Letters **18**, 202 (1967).
 - [4] R. H. Kraichnan, Tech. Rep., DTIC Document (1967).
 - [5] G. Falkovich and V. Lebedev, Physical Review E **50**, 3883 (1994).
 - [6] V. E. Zakharov, V. S. Lvov, and G. Falkovich, *Kolmogorov Spectra of Turbulence I: Wave turbulence* (Springer-Verlag, New York, 1992).
 - [7] C. Sulem and P. L. Sulem, *Nonlinear Schrödinger Equations: Self-Focusing and Wave Collapse* (World Scientific, New York, 1999).
 - [8] L. P. Pitaevskii and S. Stringari, *Bose-Einstein Condensation* (Clarendon, Oxford, 2003).
 - [9] S. Dyachenko, A. C. Newell, A. Pushkarev, and V. E. Zakharov, Physica D **57**, 96 (1992).
 - [10] A. Dyachenko and G. Falkovich, Phys. Rev. E **54**, 5095 (1996).
 - [11] G. Falkovich, Physics of Fluids **6**, 1411 (1994).
 - [12] V. M. Malkin, Physical review letters **76**, 4524 (1996).
 - [13] M. Abramowitz and I. A. Stegun, *Handbook of mathematical functions: with formulas, graphs, and mathematical tables*, 55 (Courier Dover Publications, 1972).
 - [14] A. Korotkevich, private communications
 - [15] <http://dlmf.nist.gov/8.7#E1>, http://en.wikipedia.org/wiki/Incomplete_gamma_function